A simple physical picture for quantum control of wave packet localization

Jianshu Cao and Kent R. Wilson
Department of Chemistry and Biochemistry, University of California, San Diego, La Jolla, California 92093-0339

(Received 9 August 1996; accepted 23 April 1997)

Based on weak field quantum control theory, a semiclassical approximation relates the characteristic parameters of the tailored light field to corresponding classical dynamical quantities and thus reveals the underlying physical basis of wave packet focusing. A coordinate-dependent two-level-system approximation is employed to further analyze the molecular dynamics induced by short laser pulses, thus leading to a simple interpretation of the observed correlation between the pulse chirp and vibrational focusing and defocusing. Though our study is presented in the context of quantum control, the conclusions are general, providing an intuitive picture of the quantum coherence of light–matter interaction and a guideline for the design of tailored laser fields. © *1997 American Institute of Physics.* [S0021-9606(97)01329-9]

I. INTRODUCTION

Progress in generating tailored light pulses has made it possible to steer matter toward a specific goal, namely, to control its future.[1–8] Theory[9–14] has been developed to predict an optimal laser field to drive a quantum wave packet to a desired functional form at a chosen time and this type of quantum control has been experimentally realized.[7,8,15,16] Though various numerical algorithms of wave packet propagation can be used to implement the equations of such quantum control theory,[17–23] the numerical predictions thus obtained can be understood, as we discuss in this paper, by simple physical arguments. We present here a unified physical picture which is systematically deduced from the rigorous equations and is capable of at least qualitatively characterizing the optimal fields without resorting to the full quantum calculations.

Two distinct and supplementary approaches will be proposed, each with its own advantages and limitations. The first analysis is essentially a semiclassical approximation[24–26] to the optimal field equation for a pure state in the weak response limit. The resulting field expression consists of subpulses each corresponding to a classical trajectory which, after an expansion around its optimal stationary time, yields a Gaussian pulse with parameters given by classical dynamical quantities. The second analysis is based on a coordinate dependent two-level-system (TLS) approximation,[27–30] where the concept of an initial excited-state wave function is introduced to describe the quantum dynamical effects directly induced by a short optical pulse. The linear relation of the chirp rate and the initial momentum distribution reflects the essence of coherent control of wave packet evolution.

Several observations derived from the above two approaches clearly demonstrate the underlying correspondence between classical and quantum dynamics and thus prove instructive in understanding light–matter interaction from a classical or semiclassical point of view. We will illustrate the case of a molecule initially in the ground electronic state whose vibrational wave packet will be focused on an excited electronic state. The focusing and defocusing of wave packet s is shown to be correlated to the linear chirp rate through a simple relation.

The paper is organized as follows. A derivation of quantum control theory is sketched in Sec. II. A semiclassical analysis is presented in Sec. III and a coordinate-dependent two-level approximation in Secs. III. Using these tools, the relationship between the functional form of the light pulse, particularly in terms of chirp, and wave packet focusing and defocusing is derived in Sec. V. A discussion in Sec. VI concludes the paper.

II. QUANTUM CONTROL THEORY

We briefly review the theoretical formalism of the optimal control field for driving a wave packet to a desired target. Though most results here have been given previously,[9,13,14,17–19] a different line of derivation for the weak response results is adopted to emphasize the uniformity of the strong and weak response solutions.

Consider a molecule coupled to a time-dependent electric field via a dipole interaction. For simplicity, the molecular system consists of two electronic states, $|g\rangle$ and $|e\rangle$, described by two diabatic Hamiltonians, H_g for the ground state and $(H_e+\hbar\omega_{eg})$ for the excited state. The electric field is treated classically as

$$\epsilon(t)=E(t)e^{-i\omega_{eg}t}+E^*(t)e^{i\omega_{eg}t}, \tag{1}$$

with ω_{eg} being the transition frequency between the two states. Within the rotating wave approximation, the total Hamiltonian is given as

$$\hat{H}(t)=\hat{H}_M+\hat{H}_{\rm int}, \tag{2}$$

where the molecular term is $\hat{H}_M=\hat{H}_g|g\rangle\langle g|+\hat{H}_e|e\rangle\langle e|$ and the interaction term is $\hat{H}_{\rm int}=-\mu E^*(t)|g\rangle\langle e|-\mu E(t)|e\rangle\times\langle g|$, with μ being the transition dipole moment. The density matrix of the coupled molecule-field system obeys the Liouville equation of motion

$$\frac{d\hat{\rho}(t)}{dt}=-\frac{i}{\hbar}[\hat{H}(t),\hat{\rho}(t)]=-i\mathscr{L}(t)\hat{\rho}(t), \tag{3}$$

where $\mathscr{L}$ is the Liouville operator. It follows that the density matrix at time t_f is formally given by

$$\hat{\rho}(t)=\exp_+\left[-i\int_{t_i}^{t}\mathscr{L}(t')dt'\right]\hat{\rho}(t_i), \tag{4}$$

where the subscript+implies the time ordering of operators. The evolution of the density matrix $\hat{\rho}(t)$ as described by the above equation contains all information about the system.

In general, the target of quantum control can be specified as an operator $\hat{A}$ with the realization of control measured by the expectation value of this target operator at time l_f,[14] or explicitly

$$A(l_f)=\mathrm{Tr}[\hat{A}\hat{\rho}(t_f)]. \tag{5}$$

Our goal is to find an external field $E(t)$ which maximizes the realization of such a target under certain constraints. To this end, we can construct a functional as

$$J(t_f)=A(t_f)-\lambda\int_{t_i}^{t_f}|E(t)|^2dt, \tag{6}$$

where the Lagrange multiplier λ is introduced to constrain the total radiation energy. Rigorously, the optimization of the field can be achieved by a variational differentiation of the functional $J(t_f)$ with respect to the field, $\delta J(t_f)/\delta E^*(t)=0$, resulting in

$$\lambda E(t)=\frac{i}{\hbar}\,\mathrm{Tr}[\hat{A}(t)\mu|g\rangle\langle e|\hat{\rho}(t)-\hat{\rho}(t)\mu|g\rangle\langle e|\hat{A}(t)]. \tag{7}$$

Here, $\hat{A}(t)$ is the backward propagation of the target operator, defined as

$$\hat{A}(t)=\hat{A}(t_f)\exp_+\left[-i\int_{t}^{t_f}\mathscr{L}(t')dt'\right], \tag{8}$$

and $\hat{\rho}(t)$ is the forward propagation of the density matrix, defined as Eq. (4). In deriving Eq. (7), the explicit expression of $\delta A(t_f)/\delta E^*(t)=0$ is written as

$$\delta A(t_f)/\delta E^*(t)=\mathrm{Tr}\,\hat{A}\,\exp_+\left[-i\int_{t}^{t_f}\mathscr{L}(t')dt'\right]\times\frac{i}{\hbar}\left[|g|\rangle\langle e|,\exp_+\left[-i\int_{t_i}^{t}\mathscr{L}(t')dt'\right]\hat{\rho}(t_i)\right], \tag{9}$$

in which the large bracket indicates a quantum commutator. This leads directly to the introduction of $\hat{A}(t)$ in Eq. (8) and $\hat{\rho}(t)$ in Eq. (4).

The equation for the optimal field is the central result of quantum control theory, and the way as it is written in Eq. (7) also suggests an iterative procedure to solve this field. Starting with an initial guess for the field, the right hand side of Eq. (7) is evaluated for the field and λ is chosen such that the total energy of the pulse is normalized to a given value. These two steps constitute a numerical loop and can be continued until a convergence is reached.

This procedure is particularly instructive when the right hand side of the field equation is linearized in the weak response limit. Let us assume that the initial density matrix is defined on the ground state, $\hat{\rho}_g$, and target operator is defined on the excited state, $\hat{A}_e$, then only the second term will survive the linearization. Consequently, the field equation Eq. (7) becomes

$$\lambda E(t)=\int_{t_i}^{t_f}M(t,t')E(t')dt', \tag{10}$$

where the material response function matrix M is defined as

$$M(t,t')=\frac{1}{\hbar^2}\,\mathrm{Tr}[\hat{A}_e e^{-iH_e(t_f-t')/\hbar}\times\mu e^{-iH_g t'/\hbar}\hat{\rho}_g e^{iH_g t/\hbar}\mu e^{iH_e(t_f-t)/\hbar}]. \tag{11}$$

It can be easily seen that consecutive application of the linear operation to the initial guess for the field will filter out all components of the initial field except the eigenvector corresponding to the maximum eigenvalue. Therefore, the iteration procedure for the general case is reduced to an eigenvalue solution in the weak response limit, with the eigenvalue being the yield and the eigenvector being the optimal field.[14]

Before leaving this section, a yield function[14] is introduced as a measure of how we achieve our goal, defined by

$$y=\frac{A(t_f)}{\int_{t_i}^{t_f}|E(t)|^2dt}, \tag{12}$$

which has the same value as the Lagrangian multiplier λ when evaluated for the optimal field. The meaning of this definition is self-evident: The expectation value of the target per molecular per unit pulse energy. It then follows, in the weak response limit, that for a given molecular system and a given target the optimal pulse computed from Eqs. (10) or (7) gives the maximum yield relative to any nonoptimized pulses with the same pulse energy.

III. A SEMICLASSICAL FORMULATION

To facilitate a semiclassical analysis, we first introduce a wave function version[2,17] of the quantum control theory formulated in the last section. Assume that both the initial density matrix and the final target consist of pure states: $\hat{\rho}(t_i)=\psi_i\psi_i^+|g\rangle\langle g|$ and $\hat{A}(t_f)=\phi_f\phi_f^+|e\rangle\langle e|$, (in which ϕ^+ means Hermitian) then the field Eq. (7) can be recast into

$$\lambda E(t)=\frac{i}{\hbar}\,[\,\gamma^*\langle\phi_g(t)|\mu|\psi_e(t)\rangle-\gamma\langle\psi_g(t)|\mu|\phi_e(t)\rangle]. \tag{13}$$

Here, $\psi(t)$ is a forward propagation of the target wave function

$$\psi(t)=\exp_+\left[-i\int_{t_i}^{t}\hat{H}(t')dt'/\hbar\right]\psi_i, \tag{14}$$

$\phi(t)$ is a backward propagation of the target wave function

$$\phi(t)=\exp_+\left[i\int_t^{t_f}\hat{H}(t')dt'/\hbar\right]\phi_f. \tag{15}$$

The subscripts g and e denote the projections of the wave function on the ground-and excited states, respectively, and γ is by definition independent of time and is given as

$$\gamma=\langle\phi_e(t_f)|\psi_g(t_f)\rangle=\langle\phi_f|e^{-i\int_{t_i}^{t_f}\hat{H}(t')dt'/\hbar}|\psi_i\rangle. \tag{16}$$

In the weak response limit, only the second term of Eq. (13) remains, giving

$$E(t)=\langle\psi_i|e^{iH_e(t_f-t)/\hbar}|\phi_f\rangle, \tag{17}$$

where ψ_i is the initial ground state wave function, ϕ_f is the final excited state wave function, and the field can be normalized by the constraint on the radiation energy. Since both the target and initial wave functions are normalized, the yield function defined in Eq. (12) becomes

$$y=\frac{1}{\hbar^2}\int_{t_i}^{t_f}|E(t)|^2dt, \tag{18}$$

which indicates that the overlap of the excited state and target wave functions determines the efficacy of reaching our goal.

A simpler way to obtain the above results is to start directly from the linear optimal field equations in Liouville space, i.e., Eqs. (10) and (11). Now, under the assumption of pure states, the linearized material response function $M(t,t')$ of Eq. (10) becomes[31]

$$M(t,t')=\frac{1}{\hbar^2}\langle\psi(t)|\phi_f\rangle\langle\phi_f|\psi(t')\rangle, \tag{19}$$

in which the variables t and t' are separable. Then the optimal field eigenequation of Eq. (10) has a trivial solution, which is given by Eq. (17). The expectation value of the target can thus be cast explicitly as

$$\begin{aligned}A(t_f)&=\int_{t_i}^{t_f}\int_{t_i}^{t_f}E(t)M(t,t')E(t')dtdt'\\&=\frac{1}{\hbar^2}\left(\int_{t_i}^{t_f}|E(t)|^2dt\right)^2,\end{aligned} \tag{20}$$

which based on the definition in Eq. (12) leads to the expression for the yield in Eq. (18).

The simple wave function expression for the optimal field, Eq. (17), now serves as the starting point of the semiclassical analysis. We assume that both the initial and target wave functions are of the Gaussian form

$$\psi_i=\frac{1}{\sqrt{2\pi\alpha_i}}\exp\left[-\frac{(x-x_i)^2}{2\alpha_i}+i\frac{p_i(x-x_i)}{\hbar}\right] \tag{21}$$

and

$$\phi_f=\frac{1}{\sqrt{2\pi\alpha_f}}\exp\left[-\frac{(x-x_f)^2}{2\alpha_f}+i\frac{p_f(x-x_f)}{\hbar}\right], \tag{22}$$

where x_i and p_i are the position and momentum of the initial wave packet, α_i is the Gaussian width, and similar definitions hold for the target wave packet.

To proceed, the optimal field Eq. (17) can be expressed as

$$\begin{aligned}E(t)&=\langle\phi_f|e^{-iH_e\tau}|\psi_i\rangle^*\\&=\left|\int dx_1\int dx_2\ \phi_f(x_2)^+G(x_1,x_2;\tau)\psi_i(x_1)\right|^*,\end{aligned} \tag{23}$$

where $\tau=t_f-t$ and G is the Green function propagating from x_1 to x_2 within time τ. Next, we introduce the semiclassical approximation for the Green function[24–26] given by

$$G(x_1,x_2;\tau)=\sum_{st}D(x_1,x_2;\tau)\exp[iS(x_1,x_2;\tau)/\hbar], \tag{24}$$

where the subscript st stands for a summation over all possible stationary paths. The stationary path is a classical trajectory satisfying the Newton's equation of motion

$$[\Delta S/\Delta x(t')]_{st}=m\ddot{x}+\frac{\partial V}{\partial x}=0, \tag{25}$$

subject to the boundary conditions $x(0)=x_i$ and $x(\tau)=x_f$. $S(\tau)$ is the corresponding classical action evaluated with the Lagrangian $L[q(t')]$ along the stationary path

$$\begin{aligned}S(\tau)&=\int_0^\tau L[x(t'),\dot{x}(t')]dt'\\&=\int_0^\tau\{\tfrac{1}{2}\dot{x}(t')m\dot{x}(t')-V[x(t')]\}dt'.\end{aligned} \tag{26}$$

The prefactor $D(\tau)$ in Eq. (24), termed Van Vleck determinant, is defined as

$$D(\tau)=\sqrt{\frac{i}{2\pi\hbar}\frac{\partial^2S(x_1,x_2;\tau)}{\partial x_1\partial x_2}}, \tag{27}$$

which can be expressed in terms of the Jacobi matrix and the Maslov index. Further discussion on the semiclassical approximation can be found in several references.[32]

To evaluate the integrals in Eq. (23), the action is expanded as

$$\begin{aligned}S(x_1,x_2;\tau)=&S(x_i,x_f,\tau)+p_f(\tau)(x_2-x_f)-p_i(\tau)(x_1\\&-x_i)+\frac{1}{2}\left[\frac{\partial^2S}{\partial x_f^2}(x_2-x_f)^2+\frac{\partial^2S}{\partial x_i^2}(x_1-x_i)^2\right.\\&\left.+\frac{\partial^2S}{\partial x_1\partial x_f}(x_1-x_i)(x_2-x_f)\right]+\cdots,\end{aligned} \tag{28}$$

where we make use of classical relations $\partial S/\partial x_i=p_i(\tau)$ and $\partial S/\partial x_f=-p_f(\tau)$. Here, $p_f(\tau)=p_f(x_i,x_f;\tau)$ and $p_i(\tau)=p_i(x_i,x_f;\tau)$ are the final and initial momenta, respectively, of a classical trajectory starting from x_i and ending in x_f at time τ. Note that for a given set of x_i and x_f there may exist

more than one stationary path which satisfies the fixed boundary conditions. Then, the integrals in Eq. (23) can be completed to yield

$$E(t)=\sum_{st} N(\tau)e^{-iS(\tau)/\hbar} \times \exp\{-\tfrac{1}{2}[\Delta p(\tau)]\cdot\Pi\cdot[\Delta p(\tau)]\}, \tag{29}$$

where the prefactor $N(\tau)$ is a function weakly dependent on time except near caustics and the summation is carried over multiple classical trajectories satisfying Newton's equation and the boundary conditions. Here, the two-dimensional vector and matrix are defined as: $[\Delta p(\tau)]=[p_f(\tau)-p_f, p_i(\tau)-p_i]$ and

$$\Pi=\frac{1}{\hbar^2}(I+i\alpha S_2)^{-1}\alpha, \tag{30}$$

where

$$S_2=\begin{bmatrix} \partial^2 S/\partial x_f^2 & \partial^2 S/\partial x_f \partial x_i \\ \partial^2 S/\partial x_f \partial x_i & \partial^2 S/\partial x_i^2 \end{bmatrix}, \tag{31}$$

$$\alpha=\begin{bmatrix} \alpha_f & 0 \\ 0 & \alpha_i \end{bmatrix}, \tag{32}$$

and I is a two-dimensional identity matrix.

As there are generic difficulties associated with the nonuniform semiclassical approximation (24), the field Eq. (29) also suffers from root search problems and the divergence at caustics. Unlike an initial-value problem where the trajectory follows a unique path in phase space, the boundary-value problem requires a search for solutions to Eq. (25) which satisfy both the initial and final conditions, giving rise to the possibility of multiple solutions. Consequently, the numerical implementation of Eq. (24) poses a formidable task in many-body systems. It also happens at certain times that two or more paths may coalesce at a focal point, resulting in the divergence of the prefactor (27). In this case one can resort to more accurate uniform asymptotic approximations which assume more complicated forms.[25] Both difficulties can be avoided by making use of the initial-value formulation.[33,34] Since a qualitative analysis will serve the purpose of this paper, we do not intend to solve Eq. (2.15) numerically and shall not further discuss the complications involved in the semiclassical approximation.

If one chooses an arbitrary target, an optimal field can always be solved, but the yield as defined in Eq. (17) may not necessarily be high because of the mismatch of momenta in the exponential terms of Eq. (29). Therefore, to achieve a reasonable yield, a target should be set near the corresponding classical trajectory in phase space for a given initial position and momentum and the target time, t_f-t_i, should be larger than the time needed for the initial phase point to reach the target phase point.

Before proceeding to further discussions on the semiclassical approximation and its implications on wave packet localization, we digress to introduce the Gaussian pulse, defined as

$$E_G(t)=E_0\exp\left[-\frac{(t-t_0)^2}{2t_p^2}-i\omega_0(t-t_0)-ic\frac{(t-t_0)^2}{2}\right], \tag{33}$$

where E_0, ω_0, t_0, t_p, and c are the amplitude, the carrier frequency, the temporal center, the temporal width, and the linear chirp rate, respectively. The temporal parameters are easily understood by writing the temporal evolution of the field strength as

$$P(t)=|E(t)|^2=E_0^2\exp\left[-\frac{(t-t_0)^2}{t_p^2}\right]. \tag{34}$$

The frequency parameters are easily interpreted by taking the Fourier transformation of the field, giving the power spectrum as

$$P(\omega)=P_0\exp\left[-\frac{(\omega-\omega_0)^2 t_p^2}{(1+t_p^4c^2)}\right]=P_0\left[-\frac{(\omega-\omega_0)^2}{\Gamma^2}\right], \tag{35}$$

where the bandwidth is defined as

$$\Gamma^2=c^2t_p^2+\frac{1}{t_p^2}, \tag{36}$$

which is related to the full width half maximum of the power spectrum by $\Delta\omega_{\mathrm{FWHM}}=2\Gamma\sqrt{\ln|2}$. The Fourier transformation of the Gaussian pulse of Eq. (33) can be expressed as

$$E(\omega)=E_0\sqrt{\frac{\pi t_p^2}{1+ict_p^2}}\exp\left[i\omega t_0-\frac{(\omega-\omega_0)^2}{2\Gamma^2} -ic'\frac{(\omega-\omega_0)^2}{2}\right], \tag{37}$$

where c' is the linear chirp rate in the frequency domain, which is related to the linear chirp rate in the time domain by

$$c'=\frac{ct_p^2}{\Gamma^2}. \tag{38}$$

The chirp describes the correlation between frequency and time, which cannot be deduced from the intensity versus time or the power spectrum. Instead, the electric field can be represented in the Wigner transformation form[14]

$$F(t,\omega)=\int_{-\infty}^{\infty} d\tau\, e^{-i\omega\tau}E^*(t+\tau/2)E(t-\tau/2), \tag{39}$$

which reduces to the power spectrum $|E(\omega)|^2$ when integrated over the time variable and reduces to the intensity versus time or temporal field strength $|E(t)|^2$ when integrated over the frequency variable. Substituting the Gaussian field Eq. (33) into Eq. (39), we have

$$F_G(t,\omega)=E_0^2\exp\left\{-\frac{(t-t_0)^2}{t_p^2}-t_p^2[\omega-(\omega_0+ct-ct_0)]^2\right\}, \tag{40}$$

which clearly shows that the center of the frequency $\omega_0+c(t-t_0)$ shifts at the rate of the linear chirp c. Roughly

speaking, on the $F(t,\omega)$ contour diagram, there is a center frequency at each time, these centers form a principal axis of the contour plot, then the slope defined as the tangent formed by the time axis and this principal axis, is determined by the linear chirp rate.

Now assume that the target lies right on the classical trajectory, with τ_{st} being the time for the classical trajectory to reach the target, then $p_f(\tau_{st})=p_f$ and $p_i(\tau_{st})=p_i$. It follows that τ_{st} must correspond to a peak of the pulse and the field equation Eq. (29) can now be expanded around this optimal stationary time, resulting in

$$S(\tau)=S(\tau_{st})+\frac{\partial S}{\partial \tau_{st}}(\tau-\tau_{st})+\frac{1}{2}\frac{\partial^2 S}{\partial \tau_{st}^2}(\tau-\tau_{st})^2+\cdots, \tag{41}$$

$$p_f(\tau)-p_f=\frac{\partial p_f}{\partial \tau_{st}}(\tau-\tau_{st}), \tag{42}$$

and a similar expression for $p_i(\tau)-p_i$. Comparing with the standard definition of a Gaussian pulse in Eq. (33), we can readily identify the various terms in Eq. (29) as the temporal center $t_0=t_f-\tau_{st}$, the carrier frequency $\hbar\omega_0=-\partial S(\tau)/\partial\tau_{st}=E$, the pulse duration (or the temporal width t_p)

$$\frac{1}{t_p^2}=[\partial p(\tau_{st})]\cdot \mathrm{Re}\ \Pi\cdot[\partial p(\tau_{st})], \tag{43}$$

and the linear chirp rate

$$c=\frac{\partial^2 S}{\partial \tau_{st}^2}+[\partial p(\tau_{st})]\cdot \mathrm{Im}\ \Pi\cdot[\partial p(\tau_{st})], \tag{44}$$

where the two component vector is defined as $[\partial p(\tau_{st})]=[\partial p_f/\partial\tau_{st},\partial p_i/\partial\tau_{st}]$. The dynamical functions and their partial derivatives in this section are defined with respect to fixed boundary conditions, meaning varying τ with fixed x_i and x_f.

The approximation of quantum dynamics by classical quantities gives an intuitive picture for understanding the relation between the electric field and the quantum dynamics. To be specific, the following conclusions are discussed:

(a) As argued earlier, the energy of the wave packet is determined by the carrier frequency, $\hbar\omega_i=E$, and only targets located on the classical trajectory of energy E in phase space can be realized with the highest yield.

(b) Since each classical trajectory gives rise to a Gaussian pulse with a corresponding set of parameters given above, the optimal field can be approximated as the superposition of Gaussian pulses. In other words, the subpulses in the optimal field obtained by quantum dynamics calculations can be interpreted as multiple classical solutions.

(c) The Gaussian width given by Eq. (43) is proportional to $[\partial p_f(\tau_{st})]^2$, which in turn is related to the acceleration rate of the stationary trajectory. Therefore, to overcome the spreading, a narrow optimal pulse is preferred when the Franck–Condon region is steep.

(d) The linear chirp rate given by Eq. (44) can be simplified as $c=\partial^2 S/\partial\tau_{st}^2=-\partial E/\partial\tau_{st}$ if the second term is ignored and if the width α in Eq. (30) is small. Evidently, a pulse of positive chirp is required for focusing a cannon since more energy is needed to complete the same classical trajectory in shorter time; whereas, a pulse of negative chirp is required for focusing a reflectron since a lower-energy trajectory can reach the target in shorter time by going through a lower turning point.[35]

(e) The argument for reflectrons in (d) is not fully justified because on certain potential surfaces it may take longer to reach a lower turning point. Furthermore, if the target is put exactly at the turning point, the semiclassical approximation is not valid, as the prefactor in Eq. (27) will diverge. To this end, a different approach is presented in the next section, which serves as the theoretical basis for further studies.

All the expressions in this section can be easily generalized to a multidimensional space by adopting vector and matrix notations. Since the semiclassical approximation is employed in order to understand quantum control using classical dynamics, the conclusions presented above for a one-dimensional system will hold similarly for higher dimensionalities.

IV. A COORDINATE DEPENDENT TWO LEVEL APPROXIMATION

A two-level-system (TLS) coupled to radiation has been used as the principal model for studying various forms of light-matter interaction.[36] Despite of its simplicity, the model reduces complicated molecular systems to an analytical solvable example while capturing the main features of many physical processes. This model can be further improved by introducing a coordinate dependence into the parameters of the TLS Hamiltonian, thus reflecting the spatial inhomogeneity of realistic systems. The resulting approximation is equivalent to the frozen nuclear assumption, implying that the optical pulse is short enough that the nuclear motion can be ignored during the irradiation. Under this condition, the initial excited wave function after the pulse can be obtained in a closed form and thus the effects of the optical pulse can be directly investigated. The analytical nature of this approximation has been used earlier in studying the impulsive excitation of coherent vibrational dynamics induced by intense short pulses.[27–30,37] The explicit condition for the validity of this approximation is established by Cao and Wilson[37] and the generalization to nonstationary wave packets is presented in Sec. IV of the same reference.

Assuming a weak field, the excited part of the wave function at a later time t can be expressed as

$$\psi_e(t)=\frac{i}{\hbar}\int_{-\infty}^{t} e^{-iH_e(t-\tau)/\hbar}E(\tau)e^{-iH_g\tau/\hbar}\psi_g^i\,d\tau, \tag{45}$$

where ψ_g^i is the stationary ground-state wave function and a constant transition dipole moment is assumed, i.e., $\mu=1$. For time t much larger than the terminal time of the pulse, the excited-state wave function can be written as

$$\psi_e(t)=e^{-iH_e t/\hbar}\psi_e^i, \tag{46}$$

where the initial excited-state wave function is defined by

$$\psi_e^i = \frac{i}{\hbar} \int_{-\infty}^{\infty} e^{iH_e\tau/\hbar} E(\tau) e^{-iH_g\tau/\hbar} \psi_g^i \, d\tau. \tag{47}$$

The initial excited-state wave function ψ_e^i represents the immediate result of the pulse, excluding any further vibrational propagation on the excited-state potential.

Next, invoking the short pulse assumption so that the kinetic-energy operator can be ignored,[37] the initial excited-state wave function can be rewritten as

$$\psi_e^i(x) = \frac{1}{\hbar} \int_{-\infty}^{\infty} e^{i\omega(x)\tau} E(\tau) d\tau \; \psi_g^i(x), \tag{48}$$

where the coordinate-dependent frequency $\omega(x)$ is defined as

$$\hbar\omega(x) = V_e(x) - V_g(x). \tag{49}$$

For comparison, time-dependent perturbation theory expresses the first-order excitation wave function as $\psi_{e,n} = 1/\hbar \int_{-\infty}^{\infty} \exp[i(\omega_n - \omega_m)\tau] E(\tau) d\tau \, \psi_{g,m}$, where ψ_n and ψ_m are the eigenstates. Therefore, the change of variable from the eigenstate number n to the spatial coordinate x reflects the significant difference in the nature of the continuous wave excitation and impulsive excitation.

With this expression of the initial excited-state wave function in hand, one can readily study the coordinate and momentum distributions on the excited state due to the optical excitation, defined, respectively, as $\rho(x) = |\psi_e^i(x)|^2$ and

$$p(x) = \mathrm{Re} \, \frac{\psi_e^{i*}(x) \hat{p} \psi_e^i(x)}{|\psi_e^i(x)|^2}, \tag{50}$$

where $\hat{p}$ is the momentum operator.

As an example, assume a Gaussian form in Eq. (33) for the optical field. and substitute this Gaussian field into Eq. (48), we have

$$\psi_e^i(x) = \exp\left[- \frac{(\omega(x) - \omega_0)^2 t_p^2}{2(1 + ict_p^2)} \right] \psi_g^i(x), \tag{51}$$

which can be rewritten as $\psi(x) = a \exp(i\phi)$ with a and ϕ being the amplitude and phase, respectively. Consequently, the population distribution, given as

$$\rho(x) = a^2 = \exp\left[- \frac{(\omega(x) - \omega_0)^2}{\Gamma^2} \right] \psi_g^i(x), \tag{52}$$

is independent of the sign of the chirp, a conclusion easily verified by an analysis in eigenstate space. Furthermore, the momentum distribution is related to the linear chirp rate by

$$p(x) = \frac{\hbar}{m} \nabla\Phi(x) = \frac{\hbar}{m} s(c, t_p) \nabla\omega(x), \tag{53}$$

where ∇ is the spatial derivative. Here, the pulse shape variable, defined as

$$s(c, t_p) = \frac{ct_p^4}{(1 + c^2 t_p^4)} = \frac{ct_p^2}{\Gamma^2}, \tag{54}$$

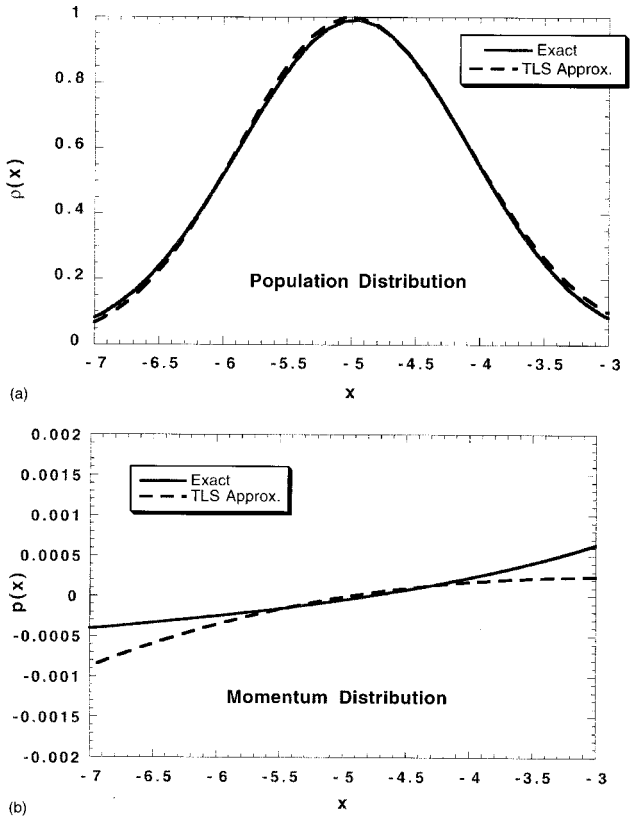

FIG. 1. A plot of the population distribution Eq. (52) and the momentum distribution Eq. (53) of the initial excited-state wave function defined by Eq. (51) for the displaced harmonic potential described in the text. The solid line is the exact quantum calculation by the splitting operator method and the dashed line is the semiclassical approximation. Note that the two level system momentum distribution in (b) diverges from the exact quantum result in the less important tails of the population distribution shown in (a).

characterizes the tailoring of the optical pulse, and is proportional to the momentum dispersion of the excited-state wave function induced by the pulse.

Usually, the Franck–Condon region is repulsive, so the spatial derivative factor in Eq. (53) is negative. Assuming a negative chirp, we then have $p(x) > 0$ if $\omega(x) > \omega_0$ and $p(x) < 0$ if $\omega(x) < \omega_0$. This result will be reversed for a positive chirp. Thus, the major effect of the chirp is to introduce a linear distribution of initial momentum which proves to be significant in quantum control. In addition, according to Eq. (53), given the linear chirp rate, the dispersion in the initial momentum distribution increases as the pulse duration. This can be better understood from the uncertainty principle as a narrow bandwidth excites a narrow wave packet in coordinate space which in turn corresponds to a broad wave packet in momentum space.

Equation (53) constitutes the central result of this section and is now put to a numerical test. Take an example of a displaced linear harmonic oscillator system defined as $H_g = p^2/2 + (x+d)^2/2$ and $H_e = p^2/2 + x^2/2$, where the displacement is $d = 5$ and unit values are assumed for mass, frequency, and the Planck constant $\hbar$. The parameters in the Gaussian pulse in Eq. (33) are given as $t_p = 1.0$, $\omega = 12.5$, and $c = 0.1$. In Fig. 1, the initial wave function approximated by

the coordinate-dependent two-level system is compared with the exact quantum calculation using the split operator method. Clearly, both the population distribution $\rho(x)$ and momentum distribution $\rho(x)$ are recovered with reasonable accuracy by the TLS approximation. More importantly, other numerical results (not shown here) confirm that the chirp of a single pulse does not effect the population distribution of the excited wave function but does induce an initial momentum distribution. Though the above argument assumes a relatively short pulse, the conclusion thus drawn is qualitatively applicable in general.

V. CHIRP AND VIBRATIONAL LOCALIZATION

There has been much recent interest in the design of laser fields for the generation of spatially squeezed or localized molecular wave packets.[31,35,38–41] In this section, we will use the concepts developed in the previous sections to investigate the interesting correlation between the chirp and vibrational localization. Recently it has been observed that the I_2 vibrational wave packet induced by an optical pulse with a negative chirp exhibits more prominent peaks and a longer delocalization time than the wave packet induced by an optical pulse with a positive chirp.

A simple explanation can be argued from the momentum distribution of the initial excited-state wave function discussed in the last section. It is known that the vibrational period of I_2 molecules on the excited surface increases with vibrational energy. As shown in Eq. (53), a negative chirp will introduce a positive initial momentum for a high-energy component and a negative initial momentum for a low-energy component so that different energy components remain better in step and thus better localized at a later time. In contrast, a positive chirp will increase the phase dispersion resulting in a broader wave packet. This conclusion will be reversed if it is the case where the vibrational period on the excited-state surface decreases with vibrational energy. In short, the sign of the chirp of the pulse which localizes or focuses a wave packet is determined by the nature of the excited-potential surface.

In order to investigate an example quantitatively, let us consider a simple control problem: The target is set to be the same as the initial ground-state wave packet. In other words, the optimal pulse is designed such that different components of the wave packet can return to its original form near the inner turning point at the same time. As already pointed out, for a general anharmonic potential, different energy components will have different vibrational periods $T(E)$ which result in a phase dispersion, $dT(E)=(dT/dE)dE$, when the wave packet returns to the turning point. On the other hand, the chirp of the optical pulse introduces a coordinate-dependent initial momentum distribution which amounts to a time delay for returning to the turning point

$$dt=\frac{p(E)}{\sqrt{2mE}}\,T, \tag{55}$$

where $p(E)$ is given by Eq. (53) as

$$p(E)=\frac{ct_p^4}{m(1+c^2t_p^4)}\,\nabla\omega\;dE. \tag{56}$$

Here, the coordinate dependence given in the last section is equivalent to the energy dependence, i.e., $\hbar\omega(x)=E$, because the coordinate x is now a classical turning point. Therefore, the optimal field should induce a time delay to match the time delay due to the energy dispersion, giving $dT(E)=dt$, or explicitly

$$s(c,t_p)=-\frac{m\sqrt{2mE}|\nabla\omega|}{T}\,\frac{dT}{dE}\equiv-\epsilon\,\frac{dT}{dE}, \tag{57}$$

where all the quantities are evaluated at the center of the Franck–Condon region corresponding to the carrier frequency, the potential gradient in position $\nabla\omega$ is always negative, and the definition of the coefficient ϵ is self evident. Since the factors contained in the coefficient ϵ are less sensitive to anharmonicity, we simply state that under the condition of $ct_p^4\gg1$ the linear chirp rate is proportional to the negative of energy dispersion.

To demonstrate the validity of the relation (57), we employ a quartic potential for the excited state

$$V_e=\tfrac{1}{2}x^2+\theta(x)gx^4, \tag{58}$$

and a displaced harmonic potential for the ground state: $V_g=1/2(x+d)^2$ with $d=5$. Here, the Heaviside function is defined as $\theta(x)=1$ for $x\geqslant0$ and $\theta(x)=0$ for $x<0$, and again unit values are assumed for mass, frequency, and the Planck constant $\hbar$. Both the initial and target wave functions are the same minimum uncertainty wave packet, $\psi_i=\phi_f=(1/\sqrt{\pi})e^{-(x+d)^2/2}$, and the target time is set at $t_f=10$. According to Eq. (57), the sign of the chirp is the same as the sign of anharmonic coefficient g in Eq. (58).

For all the examples given in this section, the quantum propagation was performed by the split operator method with a time step of 0.1 and a spatial grid of 128 points. In Fig. 2 the contour plots of the Wigner transformation of the optimal field at $t_f=10$ for the cases of $g=-0.003$, $g=0$, and $g=0.01$ are compared and clearly confirm our prediction that the slope of the optimal field takes the same sign as that of the anharmonicity.

To assess Eq. (57) quantitatively, we will investigate a simple but intriguing scenario: The target is set up at the classical turning point corresponding to the carrier frequency in the Franck–Condon region as in the last example, but the propagation time $\tau=t_f-t_i$ is not limited, i.e., $0\leqslant\tau<\infty$. This allows for an infinite number of subpulses if the excited-state vibrational wave packet contains bound eigenstates. In Fig. 3, the optimal field calculated from Eq. (17) is plotted versus $t_i=-\tau$ $(t_f=0)$ for the quartic potential defined by Eq. (58) with $g=-0.003$, which resembles a realistic molecular potential surface. The first few subpulses (counting from the right) can be easily identified until the sixth peak, after which subpulses become increasingly structured and smeared. This train of well-defined peaks corresponds to subsequent vibrational oscillations of the nuclear wave packet. In fact, extending this calculation to longer times, we have seen (not

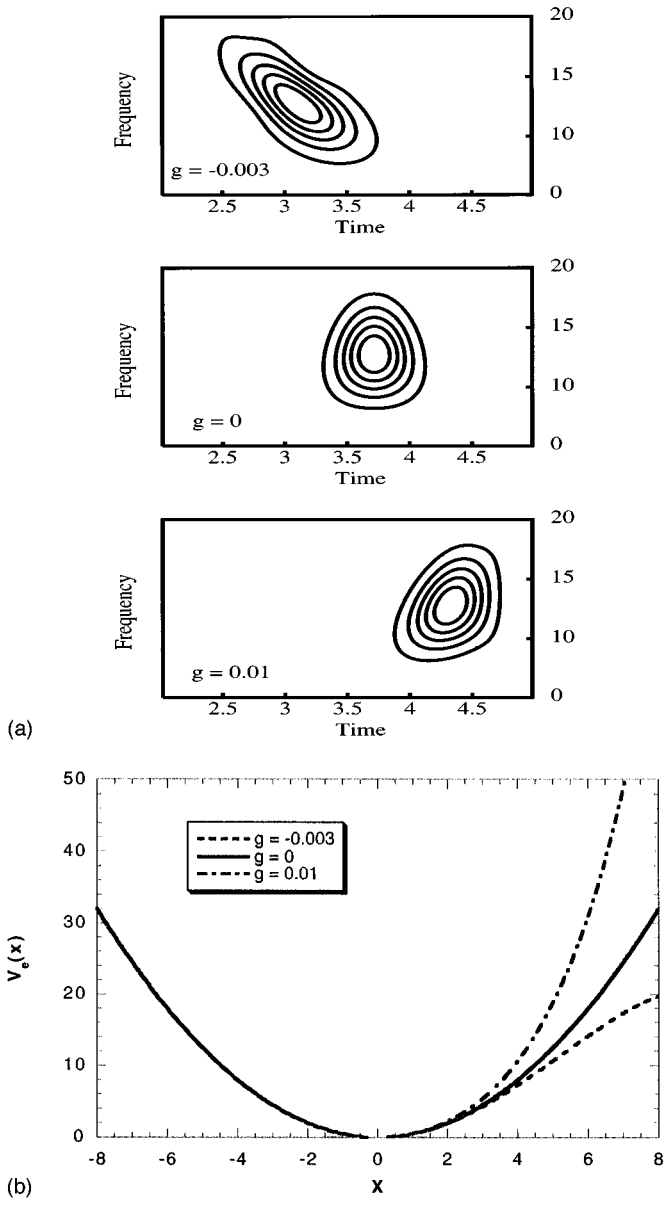

FIG. 2. Contour plots of the Wigner transformation of the optimal fields in (a) for the quartic potential of Eq. (58) with $g=-0.003$, $g=0$, and $g=0.01$, along with the plot of the quartic potential Eq. (58) in (b).

shown here) recursions in the optimal field, indicating the recurrences of vibrational motion in the same spirit as the fractional revivals observed in molecular wave packets.[41]

Following the same argument which leads to Eq. (57), it is straightforward to show that the optimal subpulse isolated from the global optimal field obeys the following relation:

$$s_n(c,t_p)=-n\epsilon\frac{dT}{dE}, \tag{59}$$

where n is the number of vibrational cycles, namely, the peak number of the optimal subpulse counted from the target time. In order words, to control a wave packet at the turning point for a target time corresponding to n oscillation periods from the center of the pulse, the shape variable of the optimal pulse should be multiplied n times. Hence, the train of

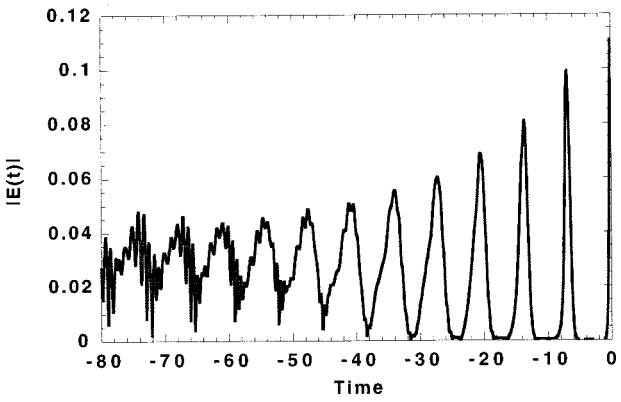

FIG. 3. The amplitude of the optimal field calculated from Eq. (17) for the quartic potential of Eq. (58) with $g=-0.003$.

subpulses isolated from the global optimal field can be employed to test the accuracy of our theory which predicts $s_n/s_1=n$. Indeed, this is exactly observed in Fig. 4 where the Wigner transformation of the optimal subpulses for $n=1-5$ are compared. Furthermore, the set of s_n calculated from its definition in Eq. (57) is listed in Table I and agrees well with the prediction of a linear increase of the shape variable s with n.

It should be mentioned, however, that increasing shape variable does not necessarily imply increasing chirp rate as $s(c,t_p)$ also depends on the Gaussian time width t_p. To this end, the semiclassical formulation in Sec. III can be used to discover the functional dependence of the chirp rate on n. From classical mechanics, one can show that the action S and time τ are linear functions of n. For a narrow Gaussian with small values of α_f or α_i, the expression for the linear chirp rate, Eq. (44) can be expanded as

$$c\approx\frac{\partial^2 S}{\partial\tau_{st}^2}+[\partial p(\tau_{st})]\cdot\alpha\cdot[\partial p(\tau_{st})], \tag{60}$$

which scales inversely with n, namely, $c\propto 1/n$. To see the consistency between this semiclassical argument and the lin-

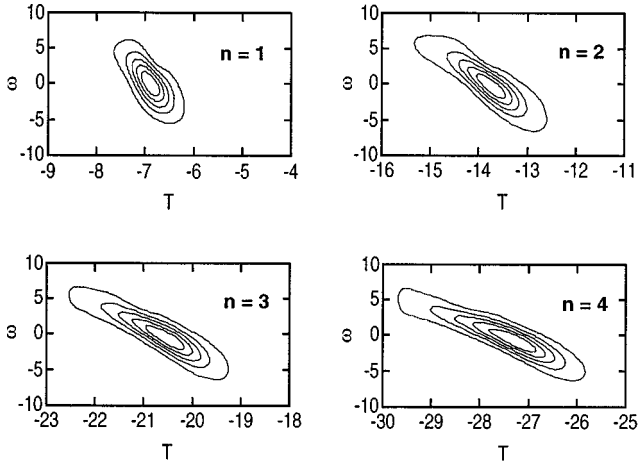

FIG. 4. Contour plots of the Wigner transformation of the optimal subpulses for $n=1,2,3,4$, counting the initial pulse ($n=1$) from the right in Fig. 3.

TABLE I. Parameters for the best Gaussian fit to the optimal subpulses.

n	c[a]	t_p[b]	Γ[c]	s[d]	r[e]
1	−8.0	0.38	16	−0.071	1.0
2	−6.0	0.62	16	−0.14	2.0
3	−4.5	0.80	15	−0.20	2.9
4	−3.2	0.92	10	−0.28	3.9
5	−2.5	1.12	8.6	−0.36	5.1

[a]c: the linear chirp rate.
[b]t_p: the pulse duration.
[c]Γ: the bandwidth, defined as $\Gamma^2=c^2t_p^2+1/t_p^2$.
[d]s: the pulse shape variable, defined as $s=ct_p^4/(1+c^2t_p^4)$.
[e]r: the ratio of the coherence variable of the nth subpulse to the coherence variable of the first subpulse, $r_n=s_n/s_1$, which is predicted to be equal to n.

ear relation (59), two limiting situations are considered as follows. First, in the case of $ct_p^4 \ll 1$, in order to have $ct_p^4 \propto n$ given $c \propto 1/n$, one must have $t_p^2 \propto n$, indicating that the pulse duration increases with time. Next, in the case of $ct_p^4 \gg 1$, we have $s \approx (1/c) \propto n$, which agrees with the scaling predicted by Eq. (59). In conclusion, a longer pulse (i.e., a larger t_p) with a smaller linear chirp rate (i.e., a smaller $|c|$) is preferred for localizing a wave packet at a later time.

Table I lists the linear chirp rate c and the time duration t_p determined by a best Gaussian fit to the exact quantum calculations. The data support our conclusions where are based on simplifying assumptions and semiclassical mechanics. In addition, in Table I, we show the frequency bandwidths, defined as $\Gamma^2=1/t_p^2+c^2t_p^2$, for the first three subpulses are similar. In fact, when the individual subpulses from the optimal pulse are examined, the spectral distribution (i.e., frequency spectra) of all the subpulses are similar, as can be seen in Fig. 4 by projecting the Wigner representations on the frequency axis (i.e., examining the frequency marginals). This is suggested by the optimal condition that the wave functions induced by different optimal subpulses should all be similar to the target wave function at the target time in order to interfere constructively, implying a similar spectrum for all optimal subpulses.

For demonstration, a pulse of the opposite chirp but otherwise with the same parameters as the optimal subpulse can be constructed as

$$E'(t-t_0)=\left[\frac{E(t_0-t)}{E(t_0)}\right]^* E(t_0), \tag{61}$$

where t_0 is the center of the subpulse, which is set zero. The transformation defined by Eq. (61) will keep the temporal shape of the pulse unchanged but flip the sign of the phase according to $\phi(t)=-\phi(-t)$. When applied to the Gaussian field Eq. (33), this transformation will change the sign of the linear chirp rate c. Comparison of excitation effects induced by a pair of opposite chirps constitutes the most important demonstration of the quantum coherence between light pulses and matter wave packets.[31,38,42–44]

Finally, the wave function of the quartic potential of Eq. (58) with $g=-0.003$ induced by the first optimal subpulse has been propagated. We then calculated $|\psi_e(0)|^2$, the probability of finding the optically excited particle at $x=0$ as a function of time, which is associated with the LIF signal from a probe window at $x=0$. The clear contrast of the results computed from the negative and positive chirps shown in Fig. 5(a) demonstrates the central role of the chirp in quantum coherence of wave packet localization. A more dramatic contrast is observed in Fig. 5(b) where the same calculation was repeated for the third subpulse isolated from Fig. 3. This observation is expected since the optimal subpulse of a larger n introduces a larger initial momentum dispersion and thus shifts the wave packet localization later in time.

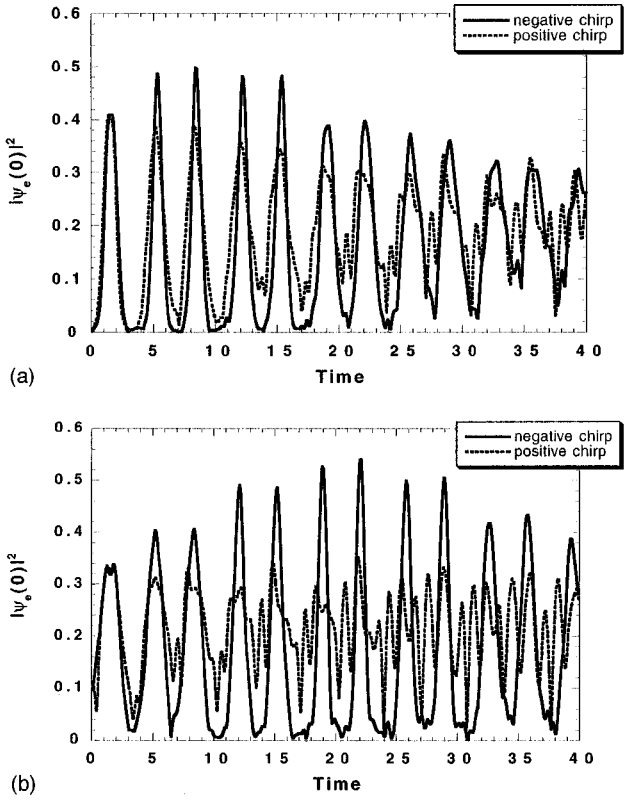

FIG. 5. The probability of finding the excited-state wave function at $x=0$ as a function of time. The solid curve corresponds to an optimal pulse with a negative chirp while the dashed curve corresponds to a similar pulse with the opposite chirp as transformed from the optimal pulse according to Eq. (61). (a) is the result of the first optimal subpulse ($n=1$) and (b) is the result of the third optimal subpulse ($n=3$).

Our example based on a specific kind of quantum control is by no means just a limiting case or an exercise. This correlation between the control pulse and the time for wave packet localization is applicable in general. Studies on realistic molecular systems in our group agree well with the analysis presented here.[16,45]

VI. CONCLUSION

A simple physical picture of optical control of wave packet localization emerges as the result of the two approximations proposed in this paper. In summary, we rephrase the major conclusions of our analysis presented in the previous sections:

(a) A short laser pulse pumps a wave packet on the excited-state potential energy surface with zero total initial momentum and a spatial spreading of position propability proportional to the pulse bandwidth Γ. To understand this nonintuitive conclusion, consider an extremely short pulse such as a delta pulse which induces a replica of the ground state wave function but cannot further suppress the width of the initial excited wave packet. In contrast, a short pulse of finite duration can not only induce all the frequency components but can also make use of the phase coherence of the components as to produce a narrower initial excited wave packet. This coherent modulation of the ground state wave function is described by the prefactor in Eq. (52) which captures the essence of the short pulse approximation.

(b) The initial momentum distribution induced by an optical pulse is determined by the shape variables $s = c\Gamma^2 t_p^2$, where the linear chip rate c is the slope on the contour plot of the Wigner transformation of the optical pulse and t_p is the temporal width of the pulse.

(c) The sign of the chirp is essential in wave packet localization. For a control time shorter than one vibrational period, the linear chirp rate can be calculated from Eq. (44); whereas for a control time longer than one vibrational period, the linear chirp rate is determined by Eq. (57).

(d) A relatively long pulse (a large time duration t_p) with a small absolute value of chirp is preferred when a wave packet is to be focused on a target to be reached after several vibrational periods.

The analysis is formulated for optimal control of a pure state in the weak response limit and some assumptions are made to simplify the derivation. Nevertheless, the results are not limited to these conditions and should hold qualitatively under more general situations. In a broader sense, the classical correspondence of quantum coherence of light–matter interaction provides an intuitive guideline for the design of laser pulses to fulfill a desired goal. In addition, the fact that our arguments based on semiclassical dynamics agree well with exact quantum calculations demonstrates the validity of semiclassical and classical approximations in the context of quantum control, thus helps explain the success of numerical quantum control simulations with classical or semiclassical algorithms.[14,20,21]

[1] S. A. Rice, Science **258**, 412 (1992).
[2] D. J. Tannor and S. A. Rice, J. Chem. Phys. **83**, 5013 (1985).
[3] A. P. Peirce, M. A. Dahleh, and H. Rabitz, Phys. Rev. A **37**, 4950 (1988).
[4] W. S. Warren, H. Rabitz, and M. Dahleh, Science **259**, 1581 (1993).
[5] P. Brumer and M. Shapiro, Faraday Discuss. Chem. Soc. **82**, 177 (1986).
[6] P. Brumer and M. Shapiro, Annu. Rev. Phys. Chem. **43**, 257 (1992).
[7] B. Kohler, J. Krause, F. Raksi, K. R. Wilson, R. M. Whitnell, V. V. Yakovlev, and Y. J. Yan, Acct. Chem. Res. **28**, 133 (1995).
[8] B. Kohler, V. V. Yakovlev, J. Che, J. L. Krause, M. Messina, K. R. Wilson, N. Schwentner, R. M. Whitnell, and Y. J. Yan, Phys. Rev. Lett. **74**, 3360 (1995).
[9] D. J. Tannor, R. Kosloff, and S. A. Rice, J. Chem. Phys. **85**, 5805 (1986).
[10] R. Kosloff, S. A. Rice, P. Gaspard, S. Tersigni, and D. J. Tannor, Chem. Phys. **139**, 201 (1989).
[11] R. S. Judson and H. Rabitz, Phys. Rev. Lett. **68**, 1500 (1992).
[12] R. Demiralp and H. Rabitz, Phys. Rev. A **47**, 809 (1993).
[13] Y. J. Yan, B. E. Kohler, R. E. Gillilan, R. M. Whitnell, K. R. Wilson, and S. Mukamel, in *Ultrafast Phenomena VIII*, edited by J.-L. Martin, A. Migus, G. A. Mourou, and A. H. Zewail (Springer, Berlin, 1993), pp. 8–12.
[14] J. L. Krause, R. M. Whitnell, K. R. Wilson, and Y. J. Yan, in *Femtosecond Chemistry*, edited by J. Manz and L. Wöste (Springer-Verlag, Weinheim, 1995), p. 743.
[15] C. J. Bardeen, J. C. K. R. Wilson, V. V. Yakovlev, P. Cong, B. Kohler, J. L. Krause, and M. Messina, J. Phys. Chem. (submitted).
[16] C. J. Bardeen, J. Che, K. R. Wilson, V. V. Yakovlev, A. P. Apkarian, C. C. Martens, R. Zadoyan, B. Kohler, and M. Messina, J. Chem. Phys. (submitted).
[17] Y. J. Yan, R. E. Gillilan, R. M. Whitnell, K. R. Wilson, and S. Mukamel, J. Phys. Chem. **97**, 2320 (1993).
[18] J. L. Krause, M. Messina, K. R. Wilson, and Y. J. Yan, J. Phys. Chem. **99**, 13736 (1995).
[19] J. Che, J. L. Krause, M. Messina, K. R. Wilson, and Y. J. Yan, J. Phys. Chem. **99**, 14949 (1995).
[20] M. Messina and K. R. Wilson, Chem. Phys. Lett. **241**, 502 (1995).
[21] M. Messina, K. R. Wilson, and J. L. Krause, J. Chem. Phys. **104**, 173 (1996).
[22] J. Che, M. Messina, K. R. Wilson, V. A. Apkarian, Z. Li, C. C. Martens, R. Zadoyan, and Y. J. Yan, J. Phys. Chem. **100**, 7873 (1996).
[23] J. Cao, M. Messina, and K. R. Wilson, J. Chem. Phys. **106**, 5236 (1997).
[24] R. P. Feynman and A. R. Hibbs, *Quantum Mechanics and Path Integrals* (McGraw-Hill, New York, 1965).
[25] L. S. Schulman, *Techniques and Applications of Path Integration* (Wiley, New York, 1986).
[26] W. H. Miller, Adv. Chem. Phys. **25**, 69 (1974).
[27] Y. J. Yan and S. Mukamel, J. Chem. Phys. **88**, 5735 (1988).
[28] J. A. Cina and T. J. Smith, J. Chem. Phys. **98**, 9211 (1993).
[29] T. J. Smith and J. A. Cina, J. Chem. Phys. **104**, 1272 (1996).
[30] U. Banin, A. Bartana, S. Ruhman, and R. Kosloff, J. Chem. Phys. **101**, 8571 (1994).
[31] J. Cao and K. R. Wilson, Phys. Rev. A (in press).
[32] V. P. Maslov and M. V. Fedoryuk, *Semiclassical Approximation in Quantum Mechanics* (Reidel, Boston, Massachusetts, 1981).
[33] G. Campolieti and P. Brumer, Phys. Rev. A **50**, 997 (1994).
[34] J. Cao and G. A. Voth, J. Chem. Phys. **104**, 273 (1996).
[35] J. L. Krause, R. M. Whitnell, K. R. Wilson, Y. J. Yan, and S. Mukamel, J. Chem. Phys. **99**, 6562 (1993).
[36] L. Allen and J. H. Eberly, *Optical Resonance and Two-Level Atoms* (Dover, New York, 1987).
[37] J. Cao and K. R. Wilson, J. Chem. Phys. **106**, 5062 (1997).
[38] I. Averbukh and M. Shapiro, Phys. Rev. A. **47**, 5086 (1993).
[39] T. J. Dunn, J. N. Sweetser, I. A. Walmsley, and C. Radzewicz, Phys. Rev. Lett. **70**, 3388 (1993).
[40] I. A. Walmsley and M. G. Raymer, Phys. Rev. A **52**, 681 (1995).
[41] M. J. J. Vrakking, D. M. Vileneuve, and A. Stolow, Phys. Rev. A (in press).
[42] N. F. Scherer, R. J. Carlson, A. Matro, M. Du, A. J. Ruggiero, V. Romero-Rochin, J. A. Cina, G. R. Fleming, and S. A. Rice, J. Chem. Phys. **95**, 1487 (1991).
[43] N. F. Scherer, A. Matro, L. D. Ziegler, M. Du, R. J. Carlson, J. A. Cina, and G. R. Fleming, J. Chem. Phys. **96**, 4180 (1992).
[44] B. Kohler, J. L. Krause, F. Raksi, C. Rose-Petruck, R. M. Whitnell, K. R. Wilson, V. V. Yakovlev, Y. J. Yan, and S. Mukamel, J. Phys. Chem. **97**, 12602 (1993).
[45] V. A. Apkarian, C. J. Bardeen, J. Che, B. Kohler, C. C. Martens, M. Messina, K. R. Wilson, V. V. Yakovlev, and R. Zadoyan, in *Ultrafast Phenomena X*, edited by J. Fujimoto, W. Zinth, P. F. Barbara, and W. H. Knox (Springer, Berlin, 1996), p. 219.